Numerical Visualization of Blast Wave Interacting with Objects

S. Dey, T. Murugan and D. Chatterjee[†]

Academy of Scientific and Innovative Research (AcSIR), CSIR-Central Mechanical Engineering Research Institute, Durgapur- 713209, India

[†]*Corresponding author, E-mail: rsdchat@yahoo.co.in*

ABSTRACT

Blast wave interaction with objects has gained attention due to military conflict and terrorist attack across the globe. Blast wave attenuating and mitigating structures are needed to be developed to protect the military vehicles and commercial buildings. In order to understand the attenuating mechanism such as the dissipation and dispersion along with the secondary effects, the blast wave interacting with three objects is examined in the present study for the diaphragm pressure ratio of 56. Here, the blast wave is generated in a short driver section open ended shock tube by solving the Euler equations using the commercial software ANSYS Fluent. It has been observed that the circular disc attenuates the blast wave more effectively compared to the cone and sphere for the same frontal area. The attenuation was lowest in the sphere and maximum in the circular disc. However, the loads acting on the sphere was more compared to the conical object. The peak load acting on the circular disc was 2.09 times more compared to the peak load acting on the conical object (cone angle 26.5°) with the same hydraulic diameter.

Keywords: Blast wave; Shock tube; Computational fluid dynamics; Blast wave attenuation; Shock loads on structures.

1. INTRODUCTION

The interaction of blast/shock wave with objects has been studied for many decades to understand the attenuation and examine the loads acting on the objects. Recently, the focus has been shifted to the development of blast mitigating structures (Igra *et al.*, 2013) due to increased volume of terrorist attack and military conflict. A clear understanding of attenuation and dissipation mechanism of the blast wave is essential for designing the efficient blast attenuating and mitigating structures. The interaction of blast wave with a circular disc, cone, and sphere is examined in the present study to understand the diffraction and reflection of blast wave during interaction along with the secondary effects such as vorticity production, shear layer instabilities, the interaction of vortices with reflected blast wave and the generation of scattered waves. Many studies were reported on the interaction of shock/blast wave with different objects, however, a comparative study of blast wave attenuation on these objects lacked in the literature.

Jialing (1999) numerically studied the interaction of blast wave with a 2-D wedge, sharp edged split plate, cylinders in a channel bend, and a moving body for shock Mach number (M) of 1.8. He compared the results with experimental interferogram and suggested for the improvement in scheme and grid resolution. Sun *et al.* (2004) examined the unsteady drag exerted on a sphere by a shock wave of M=1.22 and varying diameter of the sphere from 8 μm to 80 mm. It was found that the Euler equations resolved well the flow fields in the early unsteady interaction of a shock wave with spheres and the fluid viscosity was negligible. It was observed that the sphere experienced one order higher drag compared to the steady state during the early interaction. A transient negative drag was also noticed due to the focusing of the shock wave on the rear side of the sphere and it was dominant for high Reynolds number flows.

Kontis *et al.* (2006) captured the wave structures evolution during the interaction of shockwave with a circular cone, a sphere, a cube, and a solid wall using high-speed schlieren photography for M=1.28, 1.52, and 1.63. The scattered waves and secondary vortices generated during shockwave interaction were not shown as the focus was to examine the starting jet evolution and its interaction. There are many studies on the interaction of shock/blast wave interacting with wall available in the literature for M ≤ 2 (Kontis *et al.* 2008; Murugan and Das, 2009, Murugan *et al.*, 2016). In the present study, the interaction of blast wave with three objects namely circular disc, cone, and the sphere is examined for the shock Mach number 2.2 to understand the mechanism of blast wave reflection, diffraction, and emission of acoustic waves in addition to the calculation of loads acting on these structures.
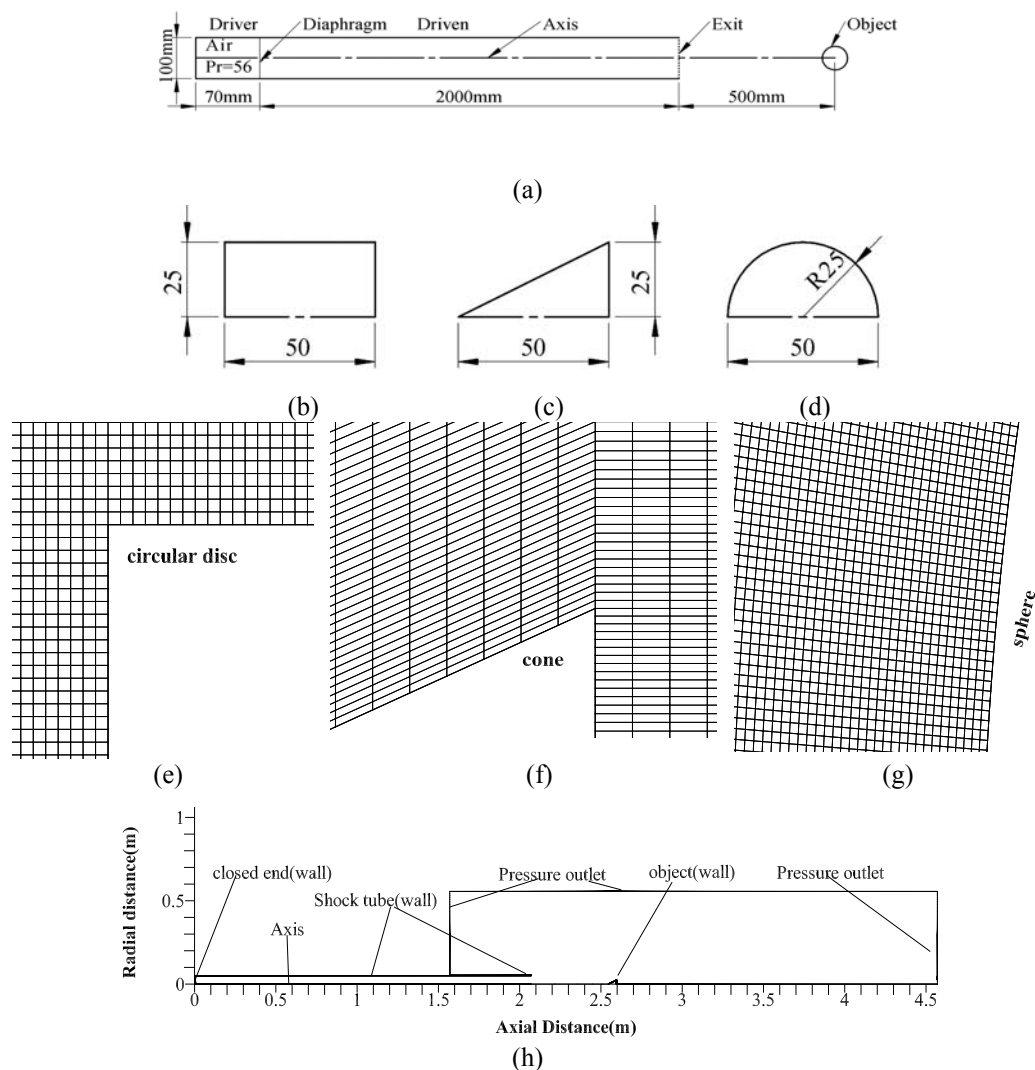
Fig. 1. (a) Shock tube (b) dimension of circular disc (c) dimension of cone (d) dimension of sphere (e) grid of circular disc (f) grid of cone (g) grid of sphere (h) flow domain with boundary conditions.

2. NUMERICAL SCHEME, INITIAL AND BOUNDARY CONDITIONS

Figure 1a shows the dimension of the shock tube driver and driven sections and the location of the objects from the shock tube exit. The numerical simulations are performed for one-half of the shock tube as the flow field is assumed to be axisymmetric. Figure 1b shows the dimensions of three different objects (circular disc, cone, and sphere) placed outside the shock tube. Though the shock/blast wave expands spherically outwards at the exit of the shock tube, its strength is larger along the axis of the shock tube due to the planar nature of the incident shock and it decreases with increase in azimuthal angle (Murugan, 2008). Hence in order to have a pseudo equal shock strength on objects during the interaction, the major dimension i.e., the height is chosen as half the diameter of the shock tube.

The shock tube, objects, and computational domain and the meshing are prepared using GAMBIT software.

There are 200 cells placed in the lateral (y) direction, and 2500 cells are placed in the flow direction (x) inside the shock tube. Here, the higher number of cells are used in the y-direction to resolve the shear layer vortices originating at the trailing jet due to Kelvin Helmholtz (K-H) instability and the effect of spatial resolution can be found in De and Murugan, 2011 and Murugan et. al., 2013. A total 0.5 million cells are used inside the shock tube. Only half the size of the objects is considered as the simulations (axisymmetric) are performed for one-half of the shock tube.

These objects are placed 5D downstream of the shock tube exit, where D is the diameter of the shock tube. The blast wave at the exit will be followed by the jet wind (Chandra *et al.*, 2012) / trailing jet (Murugan and Das, 2012). The blast wave is detached from this trailing jet after diffraction and moves along the downstream direction. The distance between the trailing jet and shock wave increases with increase in time and distance (Murugan, 2008). In order to isolate the trailing jet interaction effects, the objects are kept at 5D downstream location.

The rectangular region (4.5 D × 1D) between the shock tube exit and the circular disc is meshed with 0.64 million cells. Whereas, a total of 0.3 million cells are used for other two objects; cone and sphere. A rectangular box (1 D × 0.5 D) with the denser grid (0.1 million) is used around the disc to capture the vortices generated at corners. It has a much denser grid for the cone (0.4 million) and sphere (0.6 million) due to the complexity of the objects. Behind the disc up to a distance of 4D, 0.18 million cells are used before stretching the grid along the downstream direction. The cells are also stretched in the lateral direction away from a 1-D distance outside the shock tube. A total of 2.6, 2.5 and 2.3 million cells are used for studying the blast wave interaction with a circular disc, cone, and sphere, respectively.

The simulations are performed using commercial software ANSYS Fluent (ANSYS Fluent, 2010). Euler equations are solved in the axisymmetric form along with energy and state equations as the viscosity has the negligible role on the evolution and interaction of blast wave with objects and the subsequent vorticity production (Takayama *et al.*, 2004). The transient flow is solved with the explicit formulation. The convective terms are calculated using the AUSM flux vector splitting scheme coupled with second order upwind scheme. No-slip boundary condition is used at the shock tube walls and the surface of the objects. Pressure outlet with non-reflecting acoustic wave model is used at the open boundaries along the axial and lateral directions. The solution is initialized with an ambient pressure and temperature of 101325 N/m^2 and 303 K everywhere. The temperature is chosen based on the average temperature in our laboratory in summer. Then, the driver section is patched with the pressure of 56 times the ambient pressure before calculating the solution.

3. RESULTS AND DISCUSSION

Figure 2 shows the pressure history obtained inside and outside the shock tube at six different locations for a diaphragm pressure ratio (PR) of 56 where x = 0 represents the exit of the shock tube. At x = -1.57, a sharp rise in pressure is followed by a constant pressure before it decays exponentially. The sharp pressure rise is followed by an exponential decay similar to the blast wave as observed at x = -0.03. The interaction of expansion waves reflecting from the rear end of the shock tube with incident shock wave causes a continuous reduction in pressure along the downstream direction (Murugan, 2008; Chandra *et al.*, 2012). A nondimensional peak over pressure of 5.3 at x = -1.57 is reduced to 5 at the shock tube exit. The spherical expansion of a planar shock wave at the exit causes a huge reduction in the peak over pressure. The shock Mach number (M) inside the tube at x = -1.57 is 2.2, and it reduces gradually and becomes 2.1 at the exit. After diffraction at the exit, it reaches to a value of 1.15 and the nondimensional peak pressure is 1.4 before interacting with three objects placed at x/D = 5, where D represents the diameter of the shock tube.

Figure 3 shows the evolution of trailing jet and the interaction of blast wave with a circular disc, cone and sphere kept at x/D= 5. The objects are kept at this position to study the interaction of isolated blast wave. The diffraction of blast wave at the shock tube exit and the subsequent flow development and shock cell structure evolution for different PR up to 15 are discussed both experimentally and numerically in many earlier studies (Sun and Takayama, 2003; Murugan, 2008; Murugan *et al.*, 2013). Further, the mechanism of counter rotating vortices formation originating from Mach disc is well established (Dora el al., 2014; Murugan *et al.*, 2018). Here the PR is increased to 56, and a small driver section length of 70 mm is used for obtaining the blast wave (Friedlander profile) with M> 2 at the shock tube exit. The blast wave loses its strength along the axial direction due to spherical expansion and its M reaches to 1.15 before its interaction with objects at t~0.9 ms.
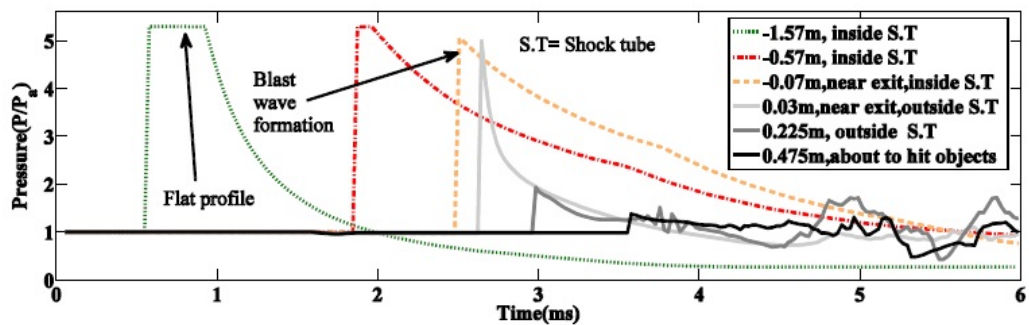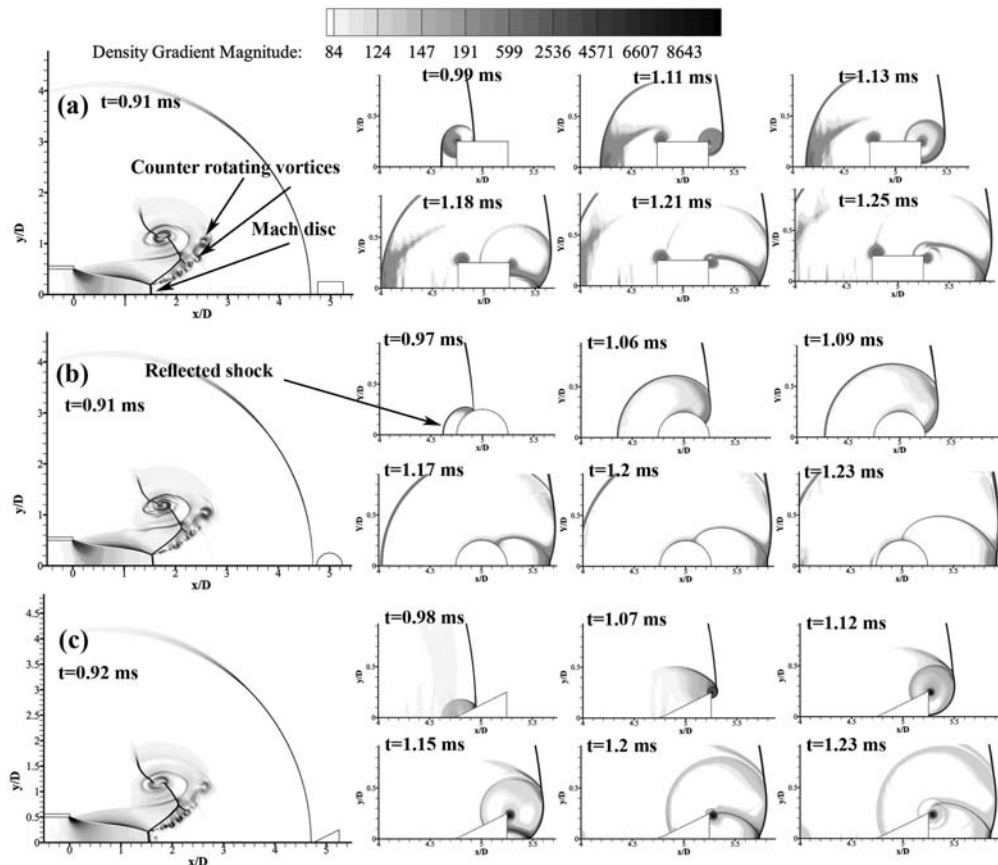

Fig. 2. Temporal variations of blast pressure inside and outside the shock tube along the axis before hitting the objects. Origin is taken at the shock tube exit and negative value indicated in the legend shows the inside shock tube distances. Time is the actual flow time.

Fig. 3. Density gradient magnitude contour plots showing the interaction of blast wave with objects at different times. Strengths of blast wave hitting the objects are same for all cases and the time t=0 corresponds to the condition when the blast wave is at the exit. (a) Circular disc (b) Sphere (c) Cone.

A portion of the incident blast wave is reflected at the forward facing step up on interacting with the disc. The blast wave is also diffracted at the forward facing sharp edge before passing over the top surface. A strong reflect shock and the formation of a slip-stream vortex at the sharp edge are seen when the blast wave passes over the front sharp edge of the disc at t=0.99 ms in Fig. 3a. This reflected shock moves along the upstream direction and expands spherically. Another slip-stream vortex is formed at the rear end of the disc due to diffraction and roll up of slipstream at the backward facing sharp edge.

The scattered waves generated during roll up and formation of these vortices are seen around the vortices from t=0.99 to 1.18 ms. These scattered waves are weak acoustic waves. The blast wave moving down behind the disc (t=0.13) gets reflected from the axis and interacts with the vortex at t=1.21 ms. During this interaction of blast wave with the vortex, the inner part of the wave gets accelerated and the outer part gets decelerated due to the angular velocity of the vortex (t=1.25 ms). The scattered waves generated during this interaction are strong acoustic waves, and they are reported in many earlier studies (Minota *et al.*, 1993; Takayama *et al.*, 1993; Murugan and Das, 2007).
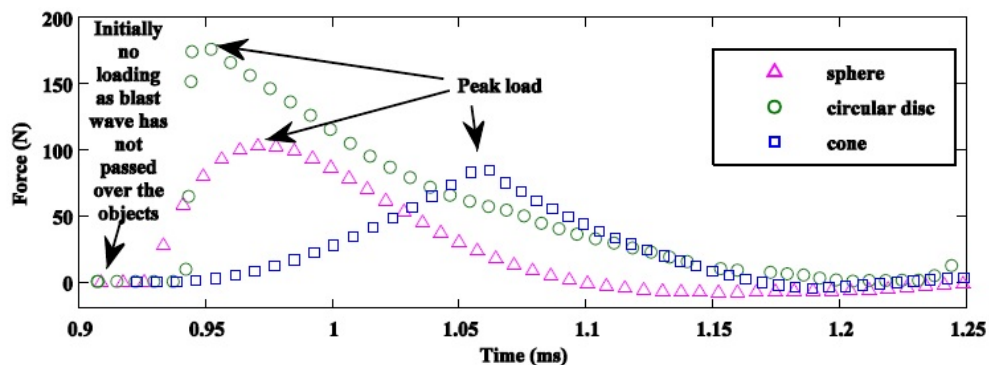
Fig. 4. Instantaneous loading on sphere, circular disc and cone when the blast wave is interacting with these objects.

Figures 3b and 3c show the evolution of blast wave interacting with sphere and cone for M=1.15. The strength of the reflected shock for the cone is much weaker compared to sphere. No vortex is formed when the blast wave passes over the sphere due to a gradual expansion of the blast wave in the rear end. However, one vortex is observed at the rear end of the cone. The instabilities arising at the slip stream and the generation of scattered waves are shown in Halder *et al.* (2013) for M=1.34 using higher order schemes. The blast wave reflected from the axis merges with the incident blast wave and form a Mach stem and a triple point which moves along the axial region.

The strength of the attenuated blast wave is identified from the curvature of the blast wave, the height of the Mach stem, and its position in the axial distance from the object. Lesser the curvature and axial position, and a larger height of the Mach stem indicate the least attenuation or a stronger blast wave in the downstream direction after the interaction. The blast wave is least attenuated after passing over the sphere as the curvature of the blast wave and the height of the Mach disc are largest compared to other two objects. It is seen from Fig. 3 that the circular disc provides stronger attenuation of blast wave compared to cone and sphere as the location of blast wave minimal is at t = 1.25 ms.

Figure 4 shows the instantaneous force acting on the objects due to blast wave loading for M=1.15. Though the hydraulic diameter is same for all three cases, the presence of a forward facing step in the case of circular disc creates a strong reflected shock and the subsequent stagnant zone in front of the disc. This causes a huge increase in force during blast wave impingement. Whereas in the case of the sphere, the force is less due to a gradual increase in frontal area. A spherical reflected wave is formed here compared to the much stronger reflected wave in the upstream direction. The reflected shock is very weak in the case of cone due to smaller flow deflection angle which causes lesser load on the conical object. For a given hydraulic diameter, the circular disc provides 2.09 times force and sphere provides 1.21 times the force acting on the cone.

4. CONCLUSION

Blast wave interacting with a circular disc, cone, and sphere is simulated numerically by solving the Euler's equations for a diaphragm pressure ratio of 56 using ANSYS Fluent. The formation of shock cell structures and counter rotating vortices originated from the secondary shear layer are observed for shock Mach number of 2.2. The evolution of blast wave over three objects and the distinct physical phenomena such as reflection, diffraction and the formation of vortices from the slip-stream are noticed along with the formation of Mach stem at the downstream direction from the objects. It is observed that the circular disc attenuates strongly the blast wave

compared to the other objects due to the presence of sharp edges. Further, blast wave loading is also observed to be maximum with circular disc and the least from the cone.

REFERENCES

ANSYS Workbench User's Guide (2010). Release 13.0, ANSYS Inc., Canonsburg, PA.

Chandra, N., Ganpule, S., Kleinschmit, N. N., Feng, R., Holmberg, A. D., Sundaramurthy, A., Selvan, V., Alai, A. (2012) Evolution of blast wave profiles in simulated air blasts: experiment and computational modeling. *Shock Waves 22*, 403–415.

De, S. and Murugan T. (2011) Numerical simulation of shock tube generated vortex: effect of numeric. *International Journal of Computational Fluid Dynamics* 345–354

Dora, C. L., Murugan T., De S. and Das D. (2014) Role of slipstream instability in formation of counter rotating vortex rings ahead of a compressible vortex ring, *Journal Fluid Mechanics, 753*. 29-48

Halder, P., De S., Sinhamahapatra K. P., Singh N. (2013) Numerical simulation of shock–vortex interaction in Schardin's problem. *Shock Waves, 23*(5): 495-504

Igra, O., Falcovitz J., Houas L., Jourdan G. (2013) Review of methods to attenuate shock / blast waves. *Progress in Aerospace Sciences, 58*. 1-35.

Jialing, J. E. (1999) Numerical Simulation of Shock (Blast) Wave Interaction with Bodies. *Communications in Nonlinear Science & Numerical Simulation, 4*(1). 1-7.

Kontis, K., An, R., Edwards, J. A. (2006) Compressible vortex-ring studies with a number of generic body configurations. *The American Institute of Aeronautics and Astronautics (AIAA) 44*. 2962-2978.

Kontis, K., An, R., Zare-Behtash, H., Kounadis, D. (2008) Head-on collision of shock wave induced vortices with solid and perforated walls. *Physics of Fluids 20*. 016104.

Minota, T. (1993) Interaction of Shock with High Speed Vortex Ring. *Fluid Dynamics Research, 12*. 335-342.

Murugan, T., and Das, D. (2007) *Experimental Investigation of the Acoustic Characteristics of Shock-Vortex Ring Interaction Process*. 13th AIAA/CEAS Aeroacoustics Conference, 21-23, Rome, Italy.

Murugan, T. (2008) *Flow and acoustic characteristics of high Mach number vortex rings during evolution and wall interaction: An experimental investigation*, PhD thesis, Indian Institute of Technology, Kanpur, India

Murugan, T., Das, D. (2009) On the Evolution of Counter Rotating Vortex Ring Formed Ahead of a Compressible Vortex Ring. *Journal of Visualization* 12. 3

Murugan, T., De, S., Dora, C. L., Das, D., Prem Kumar, P. (2013) A study of the counter rotating vortex rings interacting with the primary vortex ring in shock tube generated flows, *Fluid Dynamics Research 45* (2): 025506

Murugan, T, and S. De (2012) Numerical visualization of counter rotating vortex ring formation ahead of shock tube generated vortex ring, *Journal of Visualization, 15* (2): 97-100

Murugan, T., and Das, D., Experimental Study on a Compressible Vortex Ring in Collision with a Wall. *Journal of Visualization 15* (4), 2012, 321–332

Murugan, T., De S., Sreevatsa, A., Dutta S. (2016) Numerical Simulation of Compressible Vortex - Wall Interaction, *Shockwaves. 26* (3): 311–326

Murugan, T., Sudipta, De, Dora, C. L., Das, D., (2018) A comparative three-dimensional study of impulsive flow emanating from a shock tube for shock Mach number 1.6.. *Journal of Visualization*.

Sun, M., Takayama, K. (2003) A note on numerical simulation of vortical structures in shock diffraction. *Shock Waves* 13 (1): 25–32.

Takayama, F., Ishii, Y., Sakurai, A., Kambe, T. (1993) Self-Intensification in Shock Wave and Vortex Interaction. *Fluid dynamic research*, 12. 343-348.

Takayama, K., Saito, T., Sun, M., Tamai, K., Tanno, H., Falcovitz, J. (2004). *Unsteady drag force measurements of shock loaded bodies suspended in a vertical shock tube*. Proceedings of the 21st International Congress of Theoretical and Applied Mechanics, Warsaw, Poland.